

Supplementary Material: A Spatial Toggle Switch Drives Boundary Formation in Development, by Canela-Xandri et al.

Phase diagram and robustness analysis: analytical results

Here we proceed to analytically estimate a phase diagram in the parameter space for proper functioning of the spatial toggle switch by using a Boolean approach and assuming a 1D lattice. We focus on a subset of two cells, that comprises a boundary cell and a neighboring non-boundary cell ($i = 0$ and $i = 1$ respectively) as depicted in manuscript's Fig. 2A, embedded in a multicellular environment. To operate as a spatial toggle switch, the (asymptotic) stationary activities in these cells must satisfy,

	X_i^{activity}	Y_i^{activity}
$i = 0$	1	0
$i = 1$	0	1

(1)

Note that since the boundary population comprises two cells with “identical” genetic activity then $i = -1$ is a boundary cell and we can assume that $\tilde{Y}_{-1} = \tilde{Y}_0$. Therefore, according with Table 1, manuscript's Eqs. (1) for $i = 0$ and $i = 1$ in the steady state must read,

$$\begin{aligned}
 \dot{\tilde{X}}_0 = 0 &= \Lambda + \kappa - \tilde{X}_0, \\
 \dot{\tilde{X}}_1 = 0 &= \Lambda - \tilde{X}_1, \\
 \dot{\tilde{Y}}_0 = 0 &= -\tilde{Y}_0 + \kappa + D(\tilde{Y}_1 - \tilde{Y}_0), \\
 \dot{\tilde{Y}}_1 = 0 &= -\tilde{Y}_1 + D(\tilde{Y}_0 + \tilde{Y}_2 - 2\tilde{Y}_1).
 \end{aligned}
 \tag{2}$$

Equations for \tilde{Y} correspond to the steady state solution of the discrete and dimensionless version of the following continuous equation,

$$\dot{Y} = -\gamma_Y Y + 2k'_X \delta(x) + D_Y \nabla^2 Y.$$

This equation has been indeed proposed to model the establishment of morphogen profiles [1, 2] and its solution reads,

$$Y = \frac{k'_X}{\sqrt{D_Y \gamma_Y}} e^{-x \sqrt{\frac{\gamma_Y}{D_Y}}}.$$

That is,

$$Y_2 \simeq \frac{k'_X}{\sqrt{D_Y \gamma_Y}} e^{-2\Delta \sqrt{\frac{\gamma_Y}{D_Y}}} \iff \tilde{Y}_2 \simeq \frac{\kappa}{\sqrt{D}} e^{-\frac{2}{\sqrt{D}}}.$$

In this way, the set of equations (2) become closed, leading to,

$$\begin{aligned} \tilde{X}_0 &= \kappa + \Lambda, \\ \tilde{X}_1 &= \Lambda, \\ \tilde{Y}_0 &= \kappa \frac{D\sqrt{D}e^{-\frac{2}{\sqrt{D}}} + 2D + 1}{D^2 + 3D + 1}, \\ \tilde{Y}_1 &= \kappa \frac{\sqrt{D}(1 + D)e^{-\frac{2}{\sqrt{D}}} + D}{D^2 + 3D + 1}. \end{aligned} \tag{3}$$

Conditions for the concentration levels in boundary and non-boundary cells ($\tilde{X}_0 > 1$, $\tilde{Y}_0 > \tilde{\alpha}'$, $\tilde{X}_1 < \tilde{\beta}$, $\tilde{Y}_1 > \tilde{\alpha}'$) combined with Eqs. (3) provide the set of inequalities in terms of the model parameters that define the phase diagram as stated in the manuscript:

$$\begin{aligned} \tilde{\beta} &> \Lambda > 1 - \kappa, \\ \frac{\sqrt{D}(1 + D)e^{-\frac{2}{\sqrt{D}}} + D}{D^2 + 3D + 1} &> \frac{\tilde{\alpha}'}{\kappa}. \end{aligned} \tag{4}$$

Robustness: analytical results

Robustness to parameter variation for the values spanned in *in silico* experiments, r , can be estimated by means of the phase diagram as the ratio between the volume where toggle switch (unique and stable boundary formation) is obtained, V_{boundary} , and the total explored volume, V_{total} ,

$$r = \frac{V_{\text{boundary}}}{V_{\text{total}}}.$$

We characterize the phase diagram in terms of κ , D , and Λ where $\kappa \in [\kappa_{\min} = 0.5, \kappa_{\max} = 30]$, $D \in [D_{\min} = 0.2, D_{\max} = 10]$, and $\Lambda \in [\Lambda_{\min} = 0.01, \Lambda_{\max} = 0.5]$. In addition $\tilde{\alpha}' = 0.6$ and $\tilde{\beta} = 0.4$. Note that V_{total} simply reads,

$$V_{\text{total}} = \int dDdkd\Lambda = (D_{\max} - D_{\min}) (\kappa_{\max} - \kappa_{\min}) (\Lambda_{\max} - \Lambda_{\min}).$$

On the other hand, V_{boundary} is defined by means of the inequalities (4) that constrains the parameter space to a region $\Omega \subset V_{\text{total}}$ where boundary formation is obtained, that is,

$$V_{\text{boundary}} = \int_{\Omega} d\kappa d\Lambda dD = \int_{D_a}^{D_b} dD \int_{\kappa_a(D)}^{\kappa_b(D)} d\kappa \int_{\Lambda_a(D,\kappa)}^{\Lambda_b(D,\kappa)} d\Lambda,$$

The aforementioned inequalities do not allow for an exact solution of V_{boundary} . This is a consequence of $\kappa_a(D)$ functional form (see above) that defines a lower integration limit. However, we can bound V_{boundary} since,

$$\frac{D}{5} \geq \sqrt{D} e^{-\frac{2}{\sqrt{D}}} \geq 0.$$

That is, we can define $\kappa_a^{\pm}(D)$ such that,

$$\kappa_a^-(D) = \frac{\tilde{\alpha}'(D^2 + 3D + 1)}{D} \geq \kappa_a(D) \geq \kappa_a^+(D) = \frac{5\tilde{\alpha}'(D^2 + 3D + 1)}{D(6 + D)}.$$

As a consequence $V_{\text{boundary}}^+ > V_{\text{boundary}} > V_{\text{boundary}}^-$ where,

$$V_{\text{boundary}}^{\pm} = \int_{D_a}^{D_b} dD \int_{\kappa_a^{\pm}(D)}^{\kappa_b(D)} d\kappa \int_{\Lambda_a(D,\kappa)}^{\Lambda_b(D,\kappa)} d\Lambda,$$

- **Λ integration limits:** On one hand, we notice that if $\tilde{\alpha}' > \frac{1}{3}$ then $\kappa_a^{\pm}(D) > 1\forall D$. Thus, the inequality $\Lambda > (1 - \kappa)$ is satisfied within V_{total} and $\Lambda_a(D, \kappa) = \Lambda_{\text{min}}$. On the other hand, $\tilde{\beta} < \Lambda_{\text{max}}$ within V_{total} and therefore, since $\Lambda < \tilde{\beta}$ within Ω , $\Lambda_b(D, \kappa) = \tilde{\beta}$.
- **κ integration limits:** κ_{max} must be larger than $\kappa_a^{\pm}(D)$ within Ω for $V_{\text{boundary}}^{\pm}$ being different from zero. For the case $\kappa_a^-(D) | \kappa_a^+(D)$ this implies that $\kappa_{\text{max}} > 5\tilde{\alpha}' | \frac{5}{18} (8 + \sqrt{19}) \tilde{\alpha}'$ (the minimum value that $\kappa_a^-(D) | \kappa_a^+(D)$ can take). For the parameter sets analyzed in our simulations these conditions are granted within V_{total} (see below) and we set $\kappa_b(D) = \kappa_{\text{max}}$.
- **D integration limits for D :** The integration limits for D are determined by the intersection between the curves $\kappa_a^{\pm}(D)$ and κ_{max} . Hence, for the case $\kappa_a^-(D)$, we find that within Ω ,

$$\min\left(D_+ \left(\frac{\kappa_{\text{max}}}{\tilde{\alpha}'}\right), D_{\text{max}}\right) = D_a^- > D > \max\left(D_- \left(\frac{\kappa_{\text{max}}}{\tilde{\alpha}'}\right), D_{\text{min}}\right) = D_b^-,$$

where

$$D_{\pm}(z) = \frac{1}{2} \left[z - 3 \pm \sqrt{(z-1)(z-5)} \right].$$

Moreover, D_{\max} must be necessarily larger than $D_-(\kappa_{\max}/\tilde{\alpha}')$ within Ω . For the values explored in the phase diagram we find that $D_a^- = D_{\max}$ and $D_b^- = D_{\min}$. Likewise, for the case $\kappa_a^+(D)$, we find that within Ω ,

$$D_{\max} > D > \max \left(D'_- \left(\frac{\kappa_{\max}}{\tilde{\alpha}'} \right), D_{\min} \right) = D_b^+,$$

where

$$D'_-(z) = \frac{6z - 15 - \sqrt{125 + 4z(9z - 40)}}{2(5 - z)},$$

and the following condition must be satisfied: $D_{\max} > D'_-(\kappa_{\max}/\tilde{\alpha}')$. Since $\kappa_{\max} > 5\tilde{\alpha}'$ within V_{total} then $D_a^- = D_{\max}$ and $D_b^- = D_{\min}$.

Summarizing, $V_{\text{boundary}}^{\pm}$ is given by,

$$V_{\text{boundary}}^{\pm} = \int_{D_{\min}}^{D_{\max}} dD \int_{\kappa_a^{\pm}(D)}^{\kappa_{\max}} d\kappa \int_{\Lambda_{\min}}^{\tilde{\beta}} d\Lambda.$$

The integrals can now be analytically evaluated and leads to,

$$V_{\text{boundary}}^+ = \left(\tilde{\beta} - \Lambda_{\min} \right) \left((D_{\max} - D_{\min}) (\kappa_{\max} - 5\tilde{\alpha}') + \frac{5}{6} \tilde{\alpha}' \left(19 \ln \frac{6 + D_{\max}}{6 + D_{\min}} - \ln \frac{D_{\max}}{D_{\min}} \right) \right),$$

$$V_{\text{boundary}}^- = \left(\tilde{\beta} - \Lambda_{\min} \right) \left((D_{\max} - D_{\min}) (2\kappa_{\max} - \tilde{\alpha}' (6 + D_{\max} + D_{\min})) - 2\tilde{\alpha}' \ln \frac{D_{\max}}{D_{\min}} \right).$$

As a consequence we obtained that $0.67 > r > 0.75$.

Dishevelled lack-of-function mutant: *in silico* experiments

As predicted by the activity-vs-concentration function, Δ_{XY} , Dishevelled lack-of-function mutants are able to generate a boundary in our *in silico* experiments. However, in these mutants additional boundaries are prone to develop since the toggle switch mechanism is less robust. To illustrate this, Fig. 1S shows the steady state obtained in numerical simulations for wild-type (**A**) and Dishevelled lack-of-function (**B**) genotypic backgrounds. The simulation parameters and color codes are the same that those in manuscript's Fig. 7 with the exception of $\Lambda = 0.18$.

Dynamics in two spatial dimensions: Movie 1

The spatial toggle switch mechanism and our modeling approach can be generalized to two (or three) dimensional arrays of cells in a straightforward way. Movie 1 shows the dynamics of boundary formation in a two dimensional hexagonal lattice by means of a color density plot. Same parameters values that in manuscript's Fig. 7 were used. Color code for both expression (concentration) and activity: Notch:red and Wg:blue. Notice that in boundary cells the concentrations show color merging (purple=red+blue) whereas activities do not (toggle switch). The last frame of the movie represents the stationary state.

References

- [1] England, J. L & Cardy J. (2005) *Physical Review Letters* **94**, 078101.
- [2] Kicheva, A, Pantazis, P, Bollenbach, T, Kalaidzidis, Y, Bittig, T, Julicher, F, & Gonzalez-Gaitan, M. (2007) *Science* **315**, 521-525.

Figure legends

Figure 1S.

Wild-type (**A**) versus Dishevelled lack-of-function (**B**) genotypic backgrounds. In both cases Notch/Wingless is represented in red/blue. Left and right panels correspond to expression (concentration) and activity profiles respectively. As shown, multiple boundaries develop in the mutant case indicating the role played by Dsh in the reliability of the switching mechanism.

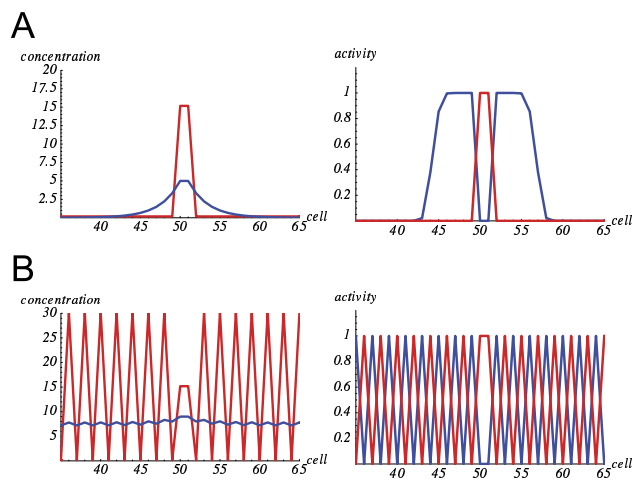


Figure 1S: